

Early-stopping for Transformer model training

Jing He* Hua Jiang[†] Cheng Li[‡] Siqian Xin[§] Shuzhen Yang[¶]

Abstract

This work introduces a novel theoretical framework grounded in Random Matrix Theory (RMT) for analyzing Transformer training dynamics. We focus on the underlying mechanisms that drive performance improvements and derive principled early-stopping criteria. Empirically, we observe that the spectral density of the shallow self-attention matrix V consistently evolves into a heavy-tailed distribution. Utilizing the PL (Power Law) fit to this matrix as a probe, we demarcate training into three stages: structural exploration, heavy-tailed structure stabilization, and convergence saturation. This staging provides guidance for preliminary stopping decisions. Crucially, we propose two consistent and validation-free criteria: a quantitative metric for heavy-tailed dynamics and a novel spectral signature indicative of convergence. The strong alignment between these criteria highlights the utility of RMT for monitoring and diagnosing the progression of Transformer model training.

Keywords: Transformer; Early stopping; Heavy-Tailed; Power-Law fitting

*Co-first Author, School of Mathematics, Shandong University, PR China, (hjing@mail.sdu.edu.cn).

[†]Co-first Author, School of Mathematics, Shandong University, PR China, (jh@mail.sdu.edu.cn).

[‡]Huawei Technologies Ltd. PR China, (cheng.li8@huawei.com). Correspondence to: Shuzhen Yang

[§]Shandong University-Zhong Tai Securities Institute for Financial Studies, Shandong University, PR China, (xin-siqian@mail.sdu.edu.cn).

[¶]Corresponding author, Shandong University-Zhong Tai Securities Institute for Financial Studies, Shandong University, PR China, (yangsz@sdu.edu.cn).

1 Introduction

Behind the remarkable success of large language models (LLMs), exemplified by the Transformer architecture, lie substantial training costs and persistent risks of overfitting (Fournier et al., 2023; Variš and Bojar, 2021). According to the well-established scaling law, the performance of an LLM is closely tied to its number of parameters, the quantity of training data, and the computational budget-factors that collectively drive the trend toward ever-larger models (Kaplan et al., 2020). Within this context, early stopping serves as a crucial regularization technique for conserving computational resources and mitigating overfitting once the validation performance saturates(Küken et al., 2025; Wu et al., 2025; Favero et al., 2025).

The classical early stopping approach relies on validation set performance (Prechelt, 2002; Muhammad et al., 2022). However, this strategy exhibits clear limitations, particularly when the training and validation distributions diverge (Taori et al., 2020) or when high-quality validation data are unavailable (Yuan et al., 2025). Heckel and Yilmaz (2020) further revealed the double descent phenomenon, suggesting that naive validation monitoring may fail to capture the true optimal stopping point. Consequently, recent research on early stopping methods has increasingly explored alternative approaches aimed at reducing or even eliminating the reliance on validation sets(Laaouach, 2025; Miseta et al., 2024; Ameryan and Schomaker, 2023). One promising direction is to focus on intrinsic model signals that more accurately reflect a model’s generalization capability. Among these, the spectral distribution of weight matrices-analyzed through the lens of Random Matrix Theory (RMT) has emerged as a powerful analytical tool.

Integrating RMT with regularization techniques enables model compression through spectral pruning without sacrificing accuracy, thereby demonstrating RMT’s potential to enhance deep learning performance (Berlyand et al., 2023, 2025). This principle of separating signal from noise provides a theoretical foundation for understanding and optimizing neural architectures. For many state-of-the-art deep networks, the spectra of weight matrices exhibit heavy-tailed (HT) behavior, well-described by a power-law distribution (Meng and Yao, 2023; Martin and Mahoney, 2021). This phenomenon is not coincidental but reflects an implicit regularization mechanism that emerges during training—known as the Heavy-Tailed Self-Regularization (HT-SR) theory (Martin and Mahoney, 2021). A key corollary of this theory is that “shape metrics” derived from spectral properties can directly predict a model’s generalization ability without access to training or test data. Subsequent studies have confirmed the effectiveness of these metrics for model selection (Yang et al., 2023) and linked them to complex learning behaviors such as “Grokking”, underscoring the potential of spectral analysis (Prakash and Martin, 2025).

From a dynamic viewpoint, HT-SR theory characterizes deep neural network (DNN) training

as an evolving process of spectral shape transformation. [Martin and Mahoney \(2021\)](#) proposed a “5+1 phase” framework to describe the progression of implicit self-regularization from weak to strong, while [Meng and Yao \(2023\)](#) later distilled this into a more practical three-stage model, revealing its close relationship to task difficulty. This insight motivates a new type of early stopping criterion: DNN training can be terminated by monitoring changes in the spectral distribution shape.

Despite the Transformer’s widespread adoption ([Vaswani et al., 2017](#)), most existing spectral studies have analyzed only the overall weight matrices of Transformer layers ([Yang et al., 2023](#); [Martin et al., 2021](#)). Few have investigated the internal spectral dynamics of the Transformer’s core component the attention mechanism specifically its Query (Q), Key (K), and Value (V) matrices. Current Transformer-oriented early stopping methods either continue to rely on validation-based monitoring ([Muhammad et al., 2022](#)) or focus on dynamic early-exit mechanisms for accelerating inference ([Küken et al., 2025](#)).

The Q, K, and V matrices play pivotal roles in information processing and representation learning within Transformer architectures. Their spectral dynamics are inherently linked to the model’s learning trajectory and ultimate generalization performance. Building upon this observation, we propose a new research direction for early stopping: leveraging the spectral distributions and heavy-tailed characteristics of Q, K, and V matrices to infer the training state and derive a novel early stopping criterion.

1. Our analysis and empirical validation reveal that the self-attention V matrix from the first encoder layer (`en.0.s.a.V`) serves as a stable and sufficient proxy for monitoring the overall training dynamics of Transformer models. Its spectral evolution exhibits both robustness and representativeness, obviating the need to track multiple matrices.
2. Based on the dynamics of this V matrix, we conceptualize Transformer training as a novel three-phase process: (i) Structural Exploration and Drastic Adjustment, (ii) Heavy-Tailed Structure Formation and Stabilization, and (iii) Performance Saturation and Convergence Plateau.
3. By fitting the spectral tail with a power-law (PL) distribution, we design a quantitative indicator that tracks the emergence of heavy-tailed structures and propose a spectral-based criterion for early stopping without requiring a validation set. This criterion effectively identifies the optimal early stopping window during the late stabilization phase.

The remainder of this paper is organized as follows. Section 2 introduces the formulation of the proposed spectral early stopping criterion. Section 3 describes the selection of the core matrix, the identification of three distinct training phases based on PL fitting, the derivation of the heavy-tailed

recognition metric, and the final early stopping criterion. Section 4 concludes the paper, and the [Appendix](#) provides additional experimental details and theoretical analyses.

2 Formulation

This paper aims to identify the training stage of Transformer models by determining the most representative core matrix (`en.0.s.a.V`) and analyzing its heavy-tailed characteristics. Based on this analysis, we establish a spectral-based early stopping criterion that guides the training process, deepens the understanding of the model’s internal dynamics, and effectively reduces training time.

To identify and analyze the most representative core matrix of the Transformer model, we begin with its fundamental components—the Query (\mathbf{Q}), Key (\mathbf{K}), and Value (\mathbf{V}) matrices. Taking the Query matrix \mathbf{Q} as an example (the same analysis applies to \mathbf{K} and \mathbf{V}), we assume it has dimensions $N \times M$, where $N \geq M$; otherwise, we analyze its transpose. The correlation matrix is defined as $\mathbf{X} = \mathbf{Q}^\top \mathbf{Q}$. Let the eigenvalues of \mathbf{X} be denoted by $\{\lambda_j\}_{j=1}^M$, where each λ_j equals the square of the corresponding singular value σ_j of \mathbf{Q} , i.e., $\lambda_j = \sigma_j^2$. The Empirical Spectral Density (ESD) of \mathbf{Q} is then defined as the empirical distribution of the eigenvalues of \mathbf{X} .

$$F^Q(x) \triangleq \frac{1}{N} \sum_{i=1}^N \mathbf{I}(\lambda_i \leq x), \quad x \in \mathbb{R}, \quad (2.1)$$

where $\mathbf{I}(\cdot)$ is the indicator function.

Following the approach of [Song et al. \(2024\)](#), we first theoretically demonstrate that even when \mathbf{Q} and \mathbf{K} are fixed during training and only \mathbf{V} is updated via gradient descent, the cross-entropy loss still converges linearly to the global optimum. This finding supports the hypothesis that the \mathbf{V} matrix plays a more central role in the model than \mathbf{Q} and \mathbf{K} .

Since the power law (PL) effectively characterizes the spectral tails of weight matrices exhibiting heavy-tailed behavior ([Meng and Yao, 2023](#); [Martin and Mahoney, 2021](#)), we perform PL fitting on all \mathbf{Q} , \mathbf{K} , and \mathbf{V} matrices to evaluate the stability and consistency of their heavy-tailed evolution. The results indicate that the \mathbf{V} matrix of the first self-attention layer (`en.0.s.a.V`) is the most representative, providing empirical validation for our hypothesis.

We further analyze the evolution of PL fitting parameters for the `en.0.s.a.V` matrix over 205 training epochs under three parameter settings. The spectral parameters exhibit highly consistent and distinct three-phase dynamics:

- 1. Structural Exploration and Drastic Adjustment:** The model transitions from random initialization, during which the weight matrix undergoes large-scale restructuring.

2. **Heavy-Tailed Structure Formation and Stabilization:** The matrix develops a stable heavy-tailed spectral structure.
3. **Performance Saturation and Convergence Plateau:** The model's primary feature-learning process is largely complete.

Using the Kolmogorov-Smirnov (KS) statistic, we show that the convergence rate of the distance between the empirical cumulative distribution function (ECDF) of the `en.0.s.a.V` matrix and the theoretical cumulative distribution function (CDF) of the PL fit is $O_p\left(\frac{1}{\sqrt{n_{\text{tail}}}}\right)$. Consequently, when the KS distance \tilde{d} between the ESD of `en.0.s.a.V` and the fitted power-law distribution falls below the threshold $d^* = \frac{C}{\sqrt{n_{\text{tail}}}}$, where C is a critical constant estimated via Monte Carlo simulation, the ESD exhibits heavy-tailed behavior. From this result, we derive the early stopping criterion

$$\max_{\text{epoch}} d^* - \tilde{d},$$

where training should be terminated when $d^* - \tilde{d}$ reaches its maximum. At this point, the model achieves the strongest implicit self-regularization and optimal generalization capacity.

By integrating the Heavy-Tailed Self-Regularization (HT-SR) framework with spectral analysis of the Transformer's core matrix `en.0.s.a.V`, we propose a robust early stopping criterion driven solely by intrinsic model signals. This approach provides deeper insight into the internal dynamics of large language models and facilitates improved model efficiency and generalization.

3 Early Stopping Mechanism Based on PL Fitting

3.1 Models setting and Datasets destails

To investigate the evolution of the Transformer's core matrices during training, we construct three Transformer variants with distinct architectural configurations, denoted as T1, T2, and T3 models.

- **T1 Model:** Consists of three encoder and decoder layers and employs a relatively narrow feed-forward network (`d_ff = 800`). The total number of parameters is 9.60M.
- **T2 Model:** Includes two encoder and decoder layers but widens the feed-forward network to (`d_ff = 1800`). The total parameter count is 9.62M, which is approximately equal to that of the **T1 Model**.

- **T3 Model:** Comprises six encoder and decoder layers and adopts the same feed-forward dimension as **T1** ($d_{ff} = 800$), resulting in a total parameter count of 19.20M.

Except for these structural variations, all other hyperparameters remain identical across the models. The complete configuration details are provided in Table 1.

Table 1: Model Architecture Configuration

Model	Param	n.layers	d_model	d_ff	n.heads
	(Param Count)	(Encoder & Decoder Layers)	(Embedding Dim)	(Feed-Forward Dim)	(Multi-Head Attn)
T1	9.60M	3	400	800	4
T2	9.62M	2	400	1800	4
T3	19.20M	6	400	800	4

To investigate the properties of the weight matrices in the Transformer model, we conduct experiments on the English-to-Chinese (En-Ch) machine translation task. The dataset statistics and relevant details are summarized in Table 2. The translation corpus is obtained from a publicly available parallel dataset¹. In the subsequent experiments, the data are divided into training and validation sets with a 9:1 ratio.

Table 2: Experimental Dataset Statistics

Translation Task	Language	Tokens (Millions)	Vocabulary Size
En-Ch (CWMT)	Chinese	11.1	16,011
	English	12.7	6,524

All experiments were conducted on the same high-performance computing platform. To eliminate the influence of hardware variability, all models were trained using identical equipment. During training, the models were optimized with the Adam optimizer, using a learning rate (lr) of 0.0001 and a batch size of 448.² The maximum sequence lengths for both the encoder and decoder

¹The English–Chinese dataset (CWMT) is available on Baidu AI Studio: <https://aistudio.baidu.com/datasetdetail/161162>

²Due to hardware constraints, we empirically found that a batch size of 448 minimizes training time while maintaining stable convergence.

(`src_len` and `tgt_len`) were set to 30. To further enhance generalization, a dropout rate of 0.2 was applied during training.

Consequently, we evaluate our approach using the following three experimental setups.

- **T1_En-Ch9.60M:** Use the T1 model trained on the En-Ch dataset.
- **T2_En-Ch9.62M:** Use the T2 model trained on the En-Ch dataset.
- **T3_En-Ch19.20M:** Use the T3 model trained on the En-Ch dataset.

3.2 Selection of Core Matrix by Power Law distribution for Transformer

For Transformer models, the attention matrices \mathbf{Q} , \mathbf{K} , and \mathbf{V} are continuously optimized during training, making them central components of the model’s parameter space. However, synchronously tracking and analyzing all \mathbf{Q} , \mathbf{K} , and \mathbf{V} matrices across every attention layer in large-scale models is computationally prohibitive. Moreover, not all matrices exhibit stable and consistent correlations with model performance throughout training. Therefore, it is necessary to identify the most representative matrix as an observation window to gain deeper insight into the internal dynamics of model training. The key question then arises: what criteria should guide the selection of such a matrix?

According to Random Matrix Theory (RMT), the spectral distribution of an untrained random matrix theoretically follows the Marchenko–Pastur (MP) distribution. However, our experiments reveal that even in the early stages of training, the weight matrices of Transformer models deviate substantially from the MP distribution. Instead, their empirical spectral densities (ESDs) exhibit prominent heavy-tailed behavior. This observation suggests that the MP distribution is not an adequate descriptor of weight-matrix properties in large language models (Prakash and Martin, 2025). To better capture this intrinsic heavy-tailed nature, we fit the ESDs of key matrices using a power-law distribution and use this fit as the criterion for identifying representative matrices. Specifically, this study evaluates the \mathbf{Q} , \mathbf{K} , and \mathbf{V} matrices along two dimensions:

- **Significance of heavy-tailed characteristics:** Identify the matrix that exhibits the strongest heavy-tailed signature via spectral analysis, thereby justifying the use of the power-law model for quantitative characterization.
- **Stability of dynamic evolution:** Select the matrix whose power-law parameters evolve most smoothly and consistently during training.

(Gurbuzbalaban et al., 2021) established that the heavy-tailed phenomenon observed in the eigenvalue spectra of deep neural network weight matrices reflects an intrinsic regularization effect of gradient-descent-based optimization. (Song et al., 2024) further elucidated the distinct optimization dynamics among different weight matrices in Transformer models under quadratic loss. Building upon these theoretical foundations, we propose Research Proposition A.1 (see Appendix A), demonstrating that analogous conclusions extend to machine translation tasks. Specifically, in a single-layer Transformer under over-parameterization (i.e., sufficiently large embedding dimension D) and proper initialization, when \mathbf{Q} and \mathbf{K} remain fixed while only \mathbf{V} undergoes gradient descent updates, the cross-entropy loss converges linearly to the global optimum. This behavior originates from the softmax kernel in the attention mechanism: while the optimization trajectories of \mathbf{Q} and \mathbf{K} are nonlinearly coupled with the kernel, the dynamics of \mathbf{V} remain approximately linear, thus providing a cleaner observational window.

Guided by this theoretical insight, we advance the hypothesis that the spectral distribution of \mathbf{V} more reliably reflects the model’s implicit regularization state. To empirically validate this hypothesis and determine which attention matrix exhibits the most pronounced heavy-tailed behavior, we design a systematic comparative analysis framework.

Following Alstott et al. (2014), we posit that if a power-law model does not significantly outperform an exponential model in fitting empirical data, there is insufficient evidence to classify the distribution as heavy-tailed. Consequently, we employ the exponential distribution as a competitive baseline and use log-likelihood ratio testing to determine which model more accurately captures heavy-tailed phenomena in the spectral data.

For a given attention matrix \mathbf{W} , the testing procedure is implemented as follows:

Step 1: Eigenvalue Selection

All eigenvalues of the correlation matrix $\mathbf{X} = \mathbf{W}^\top \mathbf{W}$ are computed. The Kolmogorov-Smirnov (KS) test is then applied to determine the optimal lower bound for model fitting, denoted as x_{\min} . Subsequent analysis focuses on the eigenvalue tail, comprising all eigenvalues satisfying $\geq x_{\min}$.

Step 2: Model Fitting

Two candidate distributions are fitted to this eigenvalue tail. Using maximum likelihood estimation (MLE), we estimate the optimal exponent α for the power-law model and the decay rate λ for the exponential model.

For the continuous power-law probability density function (PDF),

$$p(x; \alpha, x_{\min}) = \frac{\alpha - 1}{x_{\min}} \left(\frac{x}{x_{\min}} \right)^{-\alpha}, \quad (3.1)$$

where α represents the scaling parameter (or Power-Law exponent), and x_{\min} denotes the lower

threshold above which power-law behavior emerges. The MLE for α is given by:

$$\hat{\alpha} = 1 + n \left[\sum_{i=1}^n \ln \frac{x_i}{x_{\min}} \right]^{-1}. \quad (3.2)$$

Step 3: Model Comparison

The difference between the log-likelihoods of the two models, denoted as the log-likelihood ratio \mathcal{R} , is computed as:

$$\mathcal{R} = \ln \frac{\mathcal{L}_1}{\mathcal{L}_2} = \sum_{i=1}^n [\ln p_1(x_i) - \ln p_2(x_i)]. \quad (3.3)$$

If $\mathcal{R} > 0$, the data are more likely to follow a power-law distribution than an exponential one, providing evidence of heavy-tailed behavior. Otherwise, heavy-tailedness cannot be inferred.

To assess the statistical significance of this result, we adopt the procedure proposed by [Clauset et al. \(2009\)](#) to compute a p -value. If $p < 0.1$ (a commonly used significance threshold), the empirical data are considered significantly more consistent with a power-law distribution, indicating that the matrix exhibits statistically **significant heavy-tailed spectral characteristics**. Due to space limitations, detailed fitting results are presented in [Appendix B](#).

We applied this procedure to the **Q**, **K**, and **V** matrices across all attention layers of the Transformer models (T1_En-Ch9.60M, T2_En-Ch9.62M). Results concerning the **stability of dynamic evolution** are provided in [Appendix C](#).

Comprehensive experimental analysis reveals a consistent pattern: the **V** matrix in the first self-attention layer of the encoder (`en.0.s.a.v`) exhibits the most pronounced and stable heavy-tailed behavior, with clearly evolving spectral parameters and strong cross-model consistency.

3.3 Three Training Phases for Transformer model training

As discussed in Section 3.2, the `en.0.s.a.v` matrix exhibits a more pronounced heavy-tailed phenomenon, and its power-law (PL) fitting demonstrates a highly stable evolutionary pattern. This predictable evolution makes the `en.0.s.a.v` matrix an ideal observation window for uncovering the intrinsic relationship between the dynamics of this layer and the overall convergence state of the model. Based on this finding, we select the `en.0.s.a.v` matrix as the primary object of analysis to further investigate the evolution of its spectral parameters throughout training.

The analysis in Section B of the [Appendix](#) has shown that the fitted parameters of the model begin to stabilize after approximately 50 epochs. To capture this transition precisely—from an initial fluctuating phase to a convergent state—we analyze the first 205 training epochs of this layer, focusing on the evolution of its PL fitting parameters. The detailed trajectories of the fitted parameters (α and x_{\min}) across multiple epochs are presented in Figure 1.

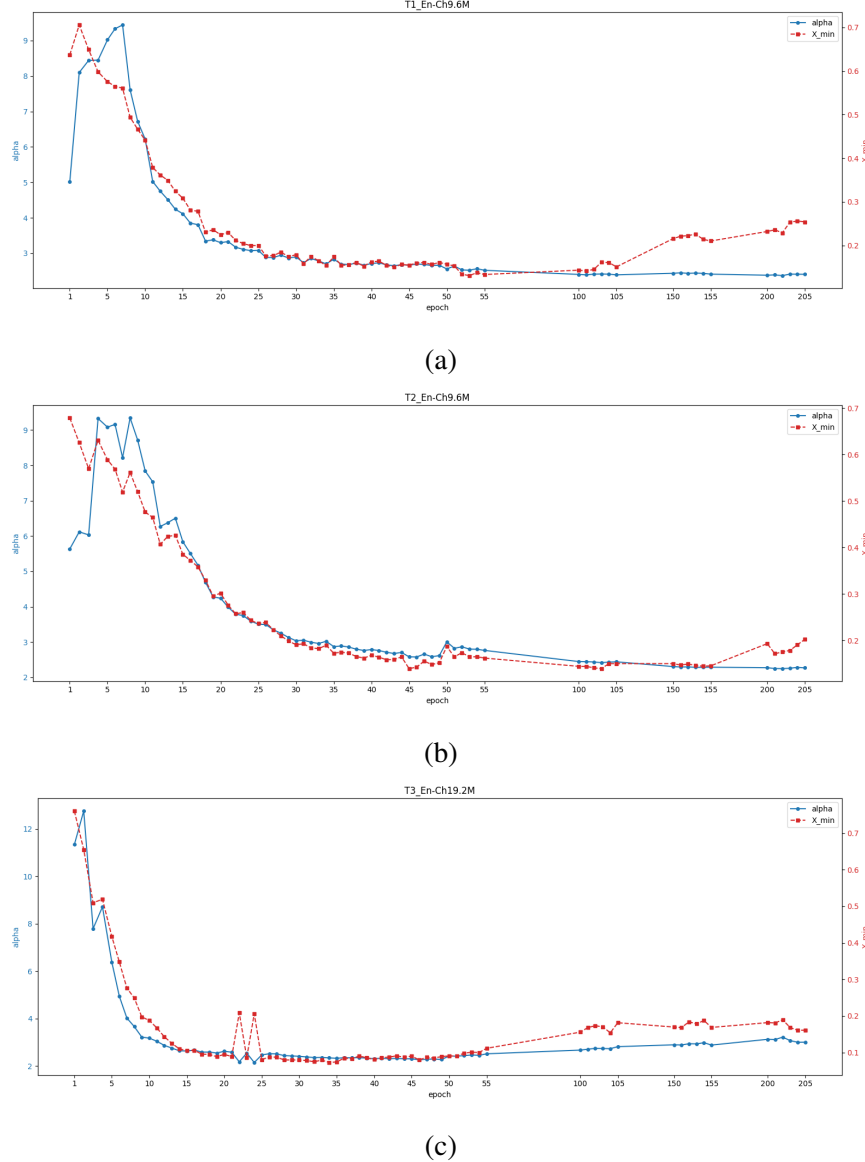


Figure 1: Evolution of α and x_{\min} for `en.0.s.a.v` matrix. Figure 1 illustrates the evolution of the PL fitting parameters for the `en.0.s.a.v` matrix, tracked across the three experimental configurations (T1_En-Ch9.60M, T2_En-Ch9.62M, T3_En-Ch19.20M) as a function of training epochs. The blue solid line (left Y-axis) represents the parameter α , while the red dashed line (right Y-axis) corresponds to the PL lower bound parameter x_{\min} .

The spectral parameters of the `en.0.s.a.v` matrix exhibit a highly consistent and distinct three-phase evolutionary dynamic across all three experimental setups.

- **Phase I: Structural Exploration and Drastic Adjustment.** During the initial training epochs, the spectral parameters undergo the most substantial dynamic changes. Both the PL exponent α and the minimum eigenvalue threshold x_{\min} remain elevated and exhibit considerable volatility. This indicates that the model is transitioning from its random initialization, with weight matrices undergoing large-scale, global structural reorganization to rapidly explore an effective feature space.
- **Phase II: Heavy-Tailed Structure Formation and Stabilization.** Following the initial exploration, the system enters a prolonged phase of stable evolution. The hallmark of this phase is the convergence of α to a low, stable value (consistently below 3 and approximately 2.5 across all experiments), maintained with high stability over hundreds of epochs. This stabilization indicates the formation of a stable heavy-tailed spectral structure within the weight matrices, a key mechanism for achieving *Implicit Regularization* in deep learning models. Concurrently, x_{\min} decreases and stabilizes at a low level (around 0.1).
- **Phase III: Performance Saturation and Convergence Plateau.** In the later training stages, the model enters a performance saturation phase. The most notable parametric change is a gradual upward trend in x_{\min} , coinciding with the increasing difficulty of achieving additional performance gains. This suggests that the primary feature-learning process has largely completed, and subsequent training primarily fine-tunes the model, indicating a convergence plateau.

Based on the evolutionary patterns illustrated in Figure 1, the training processes of the three experimental configurations can be quantitatively segmented into distinct phases. The corresponding phase durations and characteristics are summarized in the Table 3 below.

To visually examine the distinct spectral distribution characteristics across the three phases, we use the T3_En-Ch19.20M experiment as a representative case, selecting the 1st, 50th, and 200th epochs as representative time points. Figure 2 presents the Empirical Spectral Density (ESD) of the `en.0.s.a.v` matrix along with its corresponding Power-Law (PL) fit at these epochs, including a magnified view of the tail to clearly illustrate the typical spectral morphology at different training stages.

In Phase I (1st epoch, Fig. 2a), the spectral tail is steep and short. The PL fit yields a very high α value of 9.92, indicating that the weight matrix has not yet developed heavy-tailed characteristics.

Table 3: Summary of Training Phase Divisions for Each Experimental Configuration.

Experimental Configuration	Phase I:	Phase II:	Phase III:
	Structural Exploration and Drastic Adjustment	Heavy-Tailed Structure Formation and Stabilization	Performance Saturation and Convergence Plateau
T1_En-Ch 9.60M	Epochs 1–25	Epochs 26–105	Epochs 150–205
T2_En-Ch9.62M	Epochs 1–27	Epochs 28–155	Epochs 200–205
T3_En-Ch19.20M	Epochs 1–24	Epochs 25–55	Epochs 100–205

Upon entering Phase II (50th epoch, Fig. 2b), the spectrum exhibits pronounced heavy-tailed behavior, reflecting a strong HT regime. The tail extends smoothly toward larger eigenvalues and displays high dispersion. The fitted α value drops sharply to 2.44, marking the formation of a strong heavy-tailed distribution.

By Phase III (200th epoch, Fig. 2c), the heavy-tailed structure persists but is attenuated relative to Phase II, representing a weaker HT regime. Notably, the starting point of the PL fit, x_{\min} , shifts rightward, while the α value rebounds to 3.13. This contraction of the spectral tail, with fewer and smaller extreme eigenvalues, coincides with the model entering its performance saturation phase.

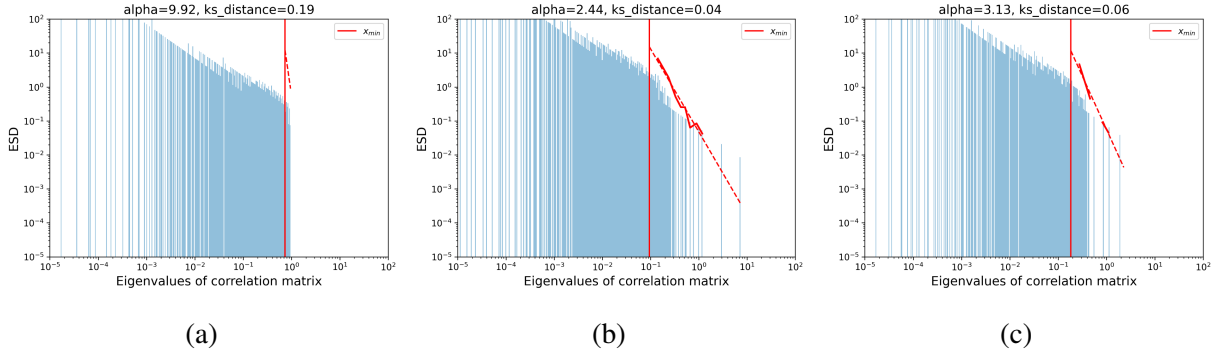


Figure 2: ESD and PL fits for the `en.0.s.a.v` matrix from the T3_En-Ch19.20M experiment at three representative training phases (1st, 50th and 200th epochs).

To further validate the correspondence between these internal spectral dynamics and external learning performance, Figure 3 shows the evolution of Loss and Accuracy values across all training epochs for the three experimental setups. During Phase I, the model exhibits the most rapid performance improvement, characterized by a sharp decline in loss and a rapid increase in accuracy. In Phase II, the rate of improvement slows, and the curves become smoother as the model

undergoes steady learning and fine-tuning. Finally, in Phase III, the performance curves plateau, with both validation loss and accuracy showing negligible further improvement, consistent with the microscopic phenomena observed in the spectral tail.

Therefore, for Transformer models, the optimal early-stopping window lies between the late portion of Phase II and the early portion of Phase III—after the heavy-tailed structure has stabilized but before the model reaches full performance saturation.

3.4 Recognition criteria for Heavy-Tail based on PL fitting

This section presents a novel spectral criterion based on PL fitting to more accurately identify the phenomenon of Heavy-Tailed period in the `en.0.s.a.v` matrix during Transformer model training. It is extremely important for us to provide early stopping criteria to guide model training and manage model performance expectations in the future. We focus on tail characteristics of `en.0.s.a.v`, specifically, the portion where the eigenvalues $x \geq x_{\min}$. All n_{tail} data points satisfying this condition can be regarded as being independently and identically drawn (i.i.d.) from an ideal PL distribution.

Based on Eq (3.1), the Cumulative Distribution Function (CDF) of this idealized power-law distribution is defined as follows,

$$F(x; \alpha, x_{\min}) = \int_{x_{\min}}^x p(t)dt = 1 - \left(\frac{x}{x_{\min}}\right)^{-\alpha+1}.$$

The Empirical Cumulative Distribution Function (ECDF) is

$$\hat{F}_{n_{\text{tail}}}(x) = \frac{1}{n_{\text{tail}}} \sum_{i=1}^{n_{\text{tail}}} I(x_i \leq x),$$

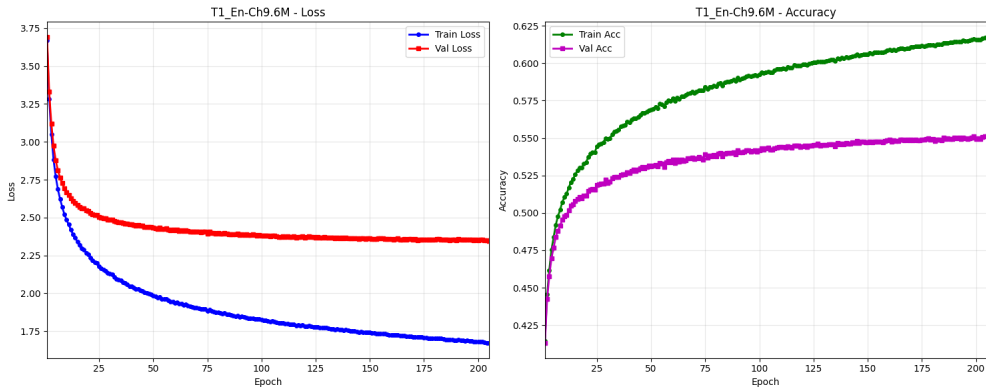
where $I(\cdot)$ is the indicator function. To quantify the agreement between the empirical eigenvalues distribution and the theoretical distribution, we employ the Kolmogorov-Smirnov (KS) statistic. The KS statistic d is defined as the maximum vertical distance between the ECDF and the theoretical CDF over the interval $x \geq x_{\min}$,

$$d = \sup_{x \geq x_{\min}} |\hat{F}_{n_{\text{tail}}}(x) - F(x; \alpha, x_{\min})|. \quad (3.4)$$

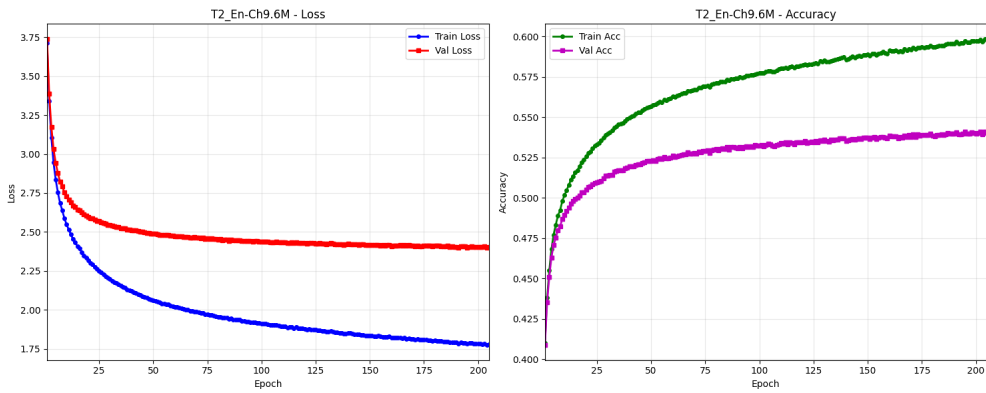
Under the null hypothesis that the data points are drawn from a power-law distribution, d converges to zero at a well-defined rate.

Lemma 3.1. *Suppose $\{X_i\}_{i=1}^n$ are generated independently from $p(x; \alpha, x_{\min}) = \frac{\alpha-1}{x_{\min}} \left(\frac{x}{x_{\min}}\right)^{-\alpha}$, then the distance in Eq (3.4) satisfies*

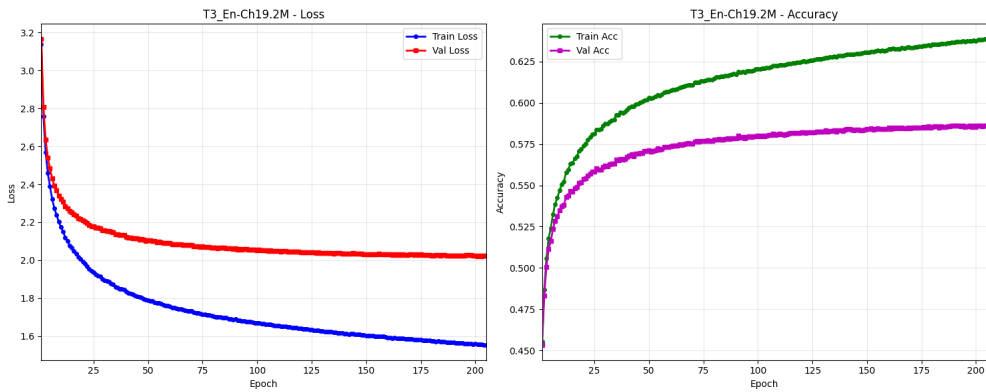
$$d = \sup_{x \geq x_{\min}} |\hat{F}_{n_{\text{tail}}}(x) - F(x; \alpha, x_{\min})| = O_p\left(\frac{1}{\sqrt{n_{\text{tail}}}}\right). \quad (3.5)$$



(a)



(b)



(c)

Figure 3: Evolution of Loss values and Accuracy values with training epochs for the three experimental setups.

(Here O_p denotes the boundedness in probability.)

Proof. We analyze the convergence rate of the KS statistic d under the assumption that the power-law exponent α is known. According to the Dvoretzky-Kiefer-Wolfowitz (DKW) inequality, a probabilistic bound exists for the maximum deviation between the ECDF and the true CDF for any finite sample. This inequality provides a rigorous characterization of the convergence rate of the KS statistic.

$$P\left(\sup_{x \in \mathbb{R}} |\hat{F}_n(x) - F(x)| > \epsilon\right) \leq 2e^{-2n\epsilon^2}. \quad (3.6)$$

Consequently, we obtain

$$P(d > \epsilon) \leq 2e^{-2n_{\text{tail}}\epsilon^2}.$$

Let $\epsilon = \frac{C}{\sqrt{n_{\text{tail}}}}$, where C is a constant. Substituting this into the inequality yields

$$P\left(d > \frac{C}{\sqrt{n_{\text{tail}}}}\right) \leq 2e^{-2n_{\text{tail}}\left(\frac{C}{\sqrt{n_{\text{tail}}}}\right)^2} = 2e^{-2C^2}.$$

Therefore, the convergence rate of the KS distance d can be expressed as

$$d = \sup_{x \geq x_{\min}} |\hat{F}_{n_{\text{tail}}}(x) - F(x; \alpha, x_{\min})| = O_p\left(\frac{1}{\sqrt{n_{\text{tail}}}}\right).$$

□

In practical applications, the PL exponent α is typically unknown and must be estimated from sample data. Maximum Likelihood Estimation (MLE) is a widely used and robust approach for estimating the parameters of a power-law distribution. The MLE for $\hat{\alpha}$ is given by

$$\hat{\alpha} = 1 + n_{\text{tail}} \left(\sum_{i=1}^{n_{\text{tail}}} \ln \frac{x_i}{x_{\min}} \right)^{-1},$$

Substituting $\hat{\alpha}$ into the CDF yields the empirical KS distance

$$\hat{d} = \sup_{x \geq x_{\min}} |\hat{F}_{n_{\text{tail}}}(x) - F(x; \hat{\alpha}, x_{\min})|. \quad (3.7)$$

The following proposition guarantees a convergence rate for the estimator \hat{d} ,

Proposition 3.1. *For the estimated distance \hat{d} in Eq (3.7), we have*

$$\hat{d} = O_p\left(\frac{1}{\sqrt{n_{\text{tail}}}}\right). \quad (3.8)$$

Proof. Consider the KS distance

$$\begin{aligned}
\hat{d} &= \sup_{x \geq x_{\min}} |\hat{F}_{n_{\text{tail}}}(x) - F(x; \hat{\alpha}, x_{\min})| \\
&\leq \sup_{x \geq x_{\min}} |\hat{F}_{n_{\text{tail}}}(x) - F(x; \alpha, x_{\min})| + \sup_{x \geq x_{\min}} |F(x; \alpha, x_{\min}) - F(x; \hat{\alpha}, x_{\min})| \\
&= d + \sup_{x \geq x_{\min}} |F(x; \alpha, x_{\min}) - F(x; \hat{\alpha}, x_{\min})|.
\end{aligned} \tag{3.9}$$

We next show that $\sup_{x \geq x_{\min}} |F(x; \alpha, x_{\min}) - F(x; \hat{\alpha}, x_{\min})| = O\left(\frac{1}{\sqrt{n_{\text{tail}}}}\right)$.

Log-likelihood function is

$$l(\alpha) = \log L(\alpha) = \sum_{i=1}^{n_{\text{tail}}} \log p(x_i; \alpha),$$

the MLE estimate $\hat{\alpha}$ is the value that maximizes $l(\alpha)$. Thus, it satisfies the first-order condition, where the score function is zero,

$$S(\hat{\alpha}) = \frac{\partial l(\alpha)}{\partial \alpha} \Big|_{\alpha=\hat{\alpha}} = \sum_{i=1}^{n_{\text{tail}}} \frac{\partial \log p(x_i; \alpha)}{\partial \alpha} \Big|_{\alpha=\hat{\alpha}} = 0.$$

Performing a first-order Taylor expansion of $S(\hat{\alpha})$ around the true parameter α_0

$$0 = S(\hat{\alpha}) \approx S(\alpha_0) + (\hat{\alpha} - \alpha_0)S'(\alpha_0),$$

$$\sqrt{n_{\text{tail}}}(\hat{\alpha} - \alpha_0) \approx \frac{\frac{1}{\sqrt{n_{\text{tail}}}}S(\alpha_0)}{-\frac{1}{n_{\text{tail}}}S'(\alpha_0)}.$$

By the Central Limit Theorem, the normalized form of the sum of i.i.d. random variables, $\frac{1}{\sqrt{n_{\text{tail}}}}S(\alpha_0)$, converges in distribution to a normal distribution with a mean of 0 and a variance equal to the Fisher Information $I(\alpha_0)$, where $I(\alpha_0) = -E\left[\frac{d^2 l(\alpha_0)}{d\alpha^2}\right]$. According to the Law of Large Numbers, the average of i.i.d. random variables, $-\frac{1}{n_{\text{tail}}}S'(\alpha_0)$, converges in probability to its expected value, which is also the Fisher Information $I(\alpha_0)$.

Combining these results, we obtain that

$$\sqrt{n_{\text{tail}}}(\hat{\alpha} - \alpha_0) \xrightarrow{d} \mathcal{N}\left(0, \frac{I(\alpha_0)}{I(\alpha_0)^2}\right) = \mathcal{N}\left(0, \frac{1}{I(\alpha_0)}\right).$$

This is the Asymptotic Normality of MLE. This conclusion indicates that $\sqrt{n_{\text{tail}}}(\hat{\alpha} - \alpha_0)$ converges to a random variable with finite variance. Therefore, $\hat{\alpha} - \alpha_0$ must scale as $1/\sqrt{n_{\text{tail}}}$ to counteract the magnifying effect of $\sqrt{n_{\text{tail}}}$, i.e., $\hat{\alpha} - \alpha_0 = O_p\left(\frac{1}{\sqrt{n_{\text{tail}}}}\right)$. Hence,

$$\begin{aligned}
F(x; \alpha, x_{\min}) - F(x; \hat{\alpha}, x_{\min}) &= \left(\frac{x}{x_{\min}}\right)^{-\hat{\alpha}+1} - \left(\frac{x}{x_{\min}}\right)^{-\alpha+1} \\
&= \left(\frac{x}{x_{\min}}\right)^{-\alpha+1} \left(\left(\frac{x}{x_{\min}}\right)^{-(\hat{\alpha}-\alpha)} - 1\right),
\end{aligned} \tag{3.10}$$

Since $\sup_{x,\alpha} \left(\frac{x}{x_{\min}}\right)^{-\alpha+1}$ is a constant and $x \geq x_{\min}$, we have

$$F(x; \alpha, x_{\min}) - F(x; \hat{\alpha}, x_{\min}) = O_p\left(\frac{1}{\sqrt{n_{\text{tail}}}}\right). \quad (3.11)$$

Hence, the convergence rate of the distance \hat{d} is

$$\hat{d} = O_p\left(\frac{1}{\sqrt{n_{\text{tail}}}}\right).$$

□

By Proposition 3.1, under the null hypothesis that the ESD of the `en.0.s.a.v` matrix follows a Power-Law distribution (i.e., exhibits Heavy-Tailed characteristics), the KS distance \hat{d} between the empirical spectral distribution and the fitted Power-Law distribution converges to 0. By defining the corresponding rejection region for the null hypothesis, we can conclude that if the ESD of the weight matrix deviates from the Power-Law form - i.e., in the absence of Heavy-Tailed characteristics- \hat{d} will no longer tend to 0. This observation leads directly to the following corollary.

Corollary 3.1. *Empirical distance \tilde{d} is the KS distance between the ESD of `en.0.s.a.v` and the fitted Power-Law distribution, i.e.,*

$$\tilde{d} = \sup_{x \geq x_{\min}} |\hat{F}_{n_{\text{tail}}}(x) - F(x; \hat{\alpha}, x_{\min})|.$$

If $\tilde{d} \leq d^$, the ESD of `en.0.s.a.v` matrix exhibits a Heavy-Tailed property; otherwise, it does not, where threshold distance d^* is*

$$d^* = \frac{C}{\sqrt{n_{\text{tail}}}}. \quad (3.12)$$

(C is a critical constant)

In the next section, we determined the value of C through Monte Carlo simulation.

3.5 Critical Constant Calibration

To establish a robust and principled value for C, we employ a Monte Carlo simulation method for calibration. This approach empirically constructs the distribution of a statistic under the null hypothesis through a large number of repeated simulations, thereby enabling the selection of an appropriate threshold. The specific procedure is as follows.

Step 1: Set Simulation Parameters

- **Theoretical Power-Law Exponent (α_0):** To ensure the robustness of the threshold C across different tail shapes, we consider several typical values for the PL exponent, e.g., $\alpha_0 = \{1.5, 2.0, 2.5, 3.0\}$.
- **Fixed Minimum Value (x_{\min}):** We adopt $x_{\min} = 0$ as determined in our primary analysis.
- **Tail Data Count (n_{tail}):** To examine the sensitivity of C to sample size, several characteristic tail sizes are tested, e.g., $n_{\text{tail}} \in \{100, 200, 300\}$.
- **Number of Monte Carlo Iterations (k):** We set $k = 10,000$ repetitions.

Step 2: Generate Synthetic Data

Synthetic datasets are generated under the null hypothesis, i.e., data perfectly follow a Power-Law distribution with the specified parameters (α_0, x_{\min}). We employ inverse transform sampling:

$$x = x_{\min} \cdot (1 - u)^{-\frac{1}{\alpha_0-1}},$$

where u is drawn uniformly from $[0, 1]$. For each combination of $(\alpha_0, n_{\text{tail}})$, this process is repeated k times to obtain k independent synthetic datasets.

Step 3: Calculate the Normalized Statistic S

For each of the k synthetic datasets, we perform the following calculations:

1. Estimate the PL exponent $\hat{\alpha}$ via Maximum Likelihood Estimation (MLE).
2. Compute the KS distance, \hat{d} , between the $\hat{F}_{n_{\text{tail}}}(x)$ of the dataset and $F(x; \hat{\alpha}, x_{\min})$ using the estimated parameter $\hat{\alpha}$.
3. Calculate the normalized KS statistic S:

$$S = \hat{d} \cdot \sqrt{n_{\text{tail}}}, \quad \text{where } \hat{d} = \sup_{x \geq x_{\min}} |\hat{F}_{n_{\text{tail}}}(x) - F(x; \hat{\alpha}, x_{\min})|.$$

Step 4: Select Threshold C

After k iterations, the resulting set of S values constitutes the empirical distribution of the normalized KS statistic under the null hypothesis.

- **Distribution Visualization:** Plot a histogram of the k values of S. This histogram provides a visual representation of the empirical probability distribution of the normalized KS statistic S under the null hypothesis.

- **Selection of the Threshold C:** Determine a “safe” upper bound from the histogram. This value, C, should exceed nearly all simulated S values, ensuring a conservative and robust threshold.

Following the steps outlined above, the results of our simulation are presented in Figure 4.

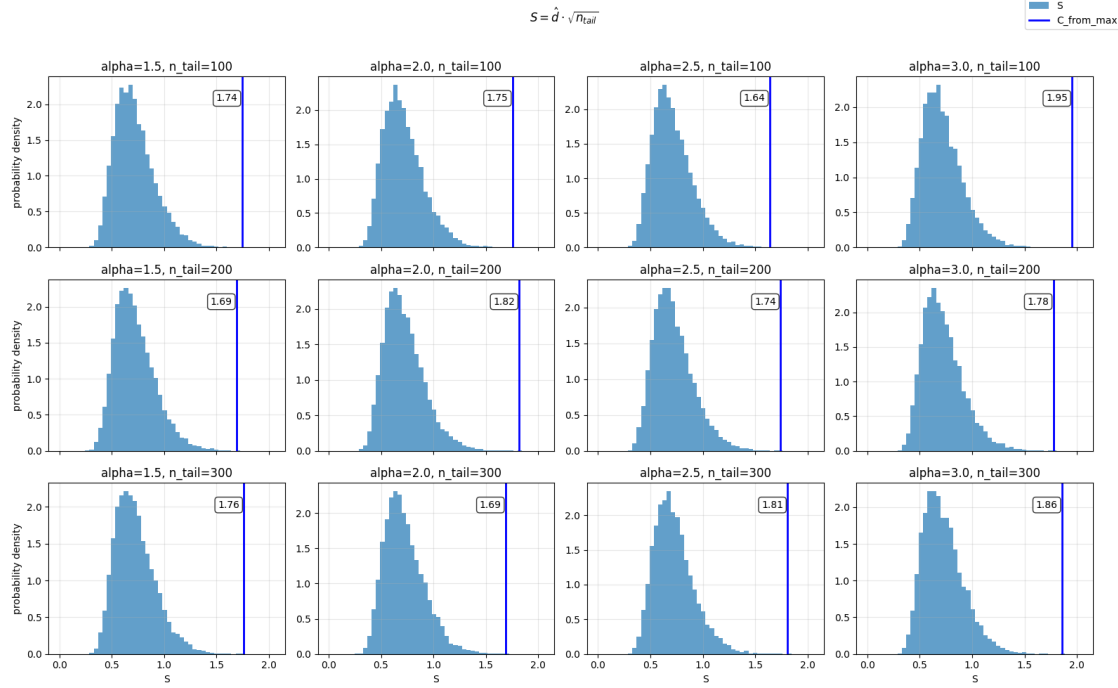


Figure 4: Monte Carlo simulation for calibrating the threshold constant C. Each subplot displays the distribution of the statistic $S = d_{\text{hat}} \cdot \sqrt{n_{\text{tail}}}$ over 10,000 runs, for different true values of α and tail sizes (n_{tail}). The vertical blue line indicates the proposed threshold.

The simulation results indicate that, across 10,000 Monte Carlo iterations for various values of α and tail data sizes (n_{tail}), the upper bound of the normalized KS statistic remains highly stable and does not exceed 2. Consequently, we select **C=2** as the critical threshold.

3.6 Early Stopping criterion and its Efficacy

In this section, we aim to construct a novel spectral criterion to identify the optimal early-stopping epoch for guiding Transformer model training. We find that the Power-Law (PL) fitting-based early-stopping criterion aligns well with the phase-partitioning-based early-stopping criteria described in Section 3.3.

According to Corollary 3.1, the Heavy-Tailed (HT) indicator, defined as the difference $d^* - \tilde{d}$ between the threshold distance and the empirical KS distance, can effectively monitor the dynamic

evolution of model training and track the formation of Heavy-Tailed spectral structures. The transition of this indicator from negative to positive values signals the entry of the spectral distribution into the Heavy-Tailed regime.

We propose an early-stopping criterion based on $\max_{\text{epoch}}\{d^* - \tilde{d}\}$, where the Heavy-Tailed (HT) indicator $d^* - d$ reaches its maximum value. This epoch is considered the optimal early-stopping point, at which the model achieves the highest degree of implicit self-regularization and the strongest generalization capability. At this point, the model’s objectives of performance optimization and training time minimization are optimally balanced.

The evolutionary trajectories of Heavy-Tailed indicator across three experimental configurations are illustrated in the figure 5. Observation of the evolutionary trajectory of the HT indicator $d^* - d$ in Figure 5 shows that, after an initial period of intense adjustment, the indicator rises rapidly, signaling the model’s entry into the Heavy-Tailed phase. Subsequently, the indicator reaches its peak and may exhibit minor fluctuations, suggesting that the Heavy-Tailed characteristics, after attaining their maximum intensity, can slightly diminish during the later stages of training.

Applying the proposed early-stopping criterion, the optimal early-stopping epochs for the three experimental configurations are identified as 100, 100, and 50, respectively. Table 4 presents a comparison of model performance at these early-stopping points against the performance achieved at the final training epoch on the validation set. The results presented in Table 4 clearly demonstrate

Table 4: Validation of Early-Stopping Strategy Effectiveness Based on Spectral Distance Metric: Performance Comparison

Model	Early-Stopping Point		Final Epoch (205)		Relative Difference	
	Loss	Accuracy	Loss	Accuracy	Diff.loss	Diff.acc
T1_En-Ch9.60M	2.3812	0.5419	2.3465	0.5512	1.479%	-1.687%
T2_En-Ch9.62M	2.4360	0.5322	2.4033	0.5402	1.361%	-1.481%
T3_En-Ch19.20M	2.1039	0.5713	2.0248	0.5861	3.907%	-1.48%

the effectiveness of the proposed early-stopping strategy. For experiments T1_En-Ch9.60M and T2_En-Ch9.62M, an additional 105 epochs of training yields a loss reduction of less than 1.5% and an accuracy improvement of less than 1.7%. In experiment T3_En-Ch19.20M, extending training by 155 epochs results in a loss reduction of less than 4% and an accuracy gain of less than 1.5%. These findings indicate that the spectral distance-based early-stopping criterion can substantially

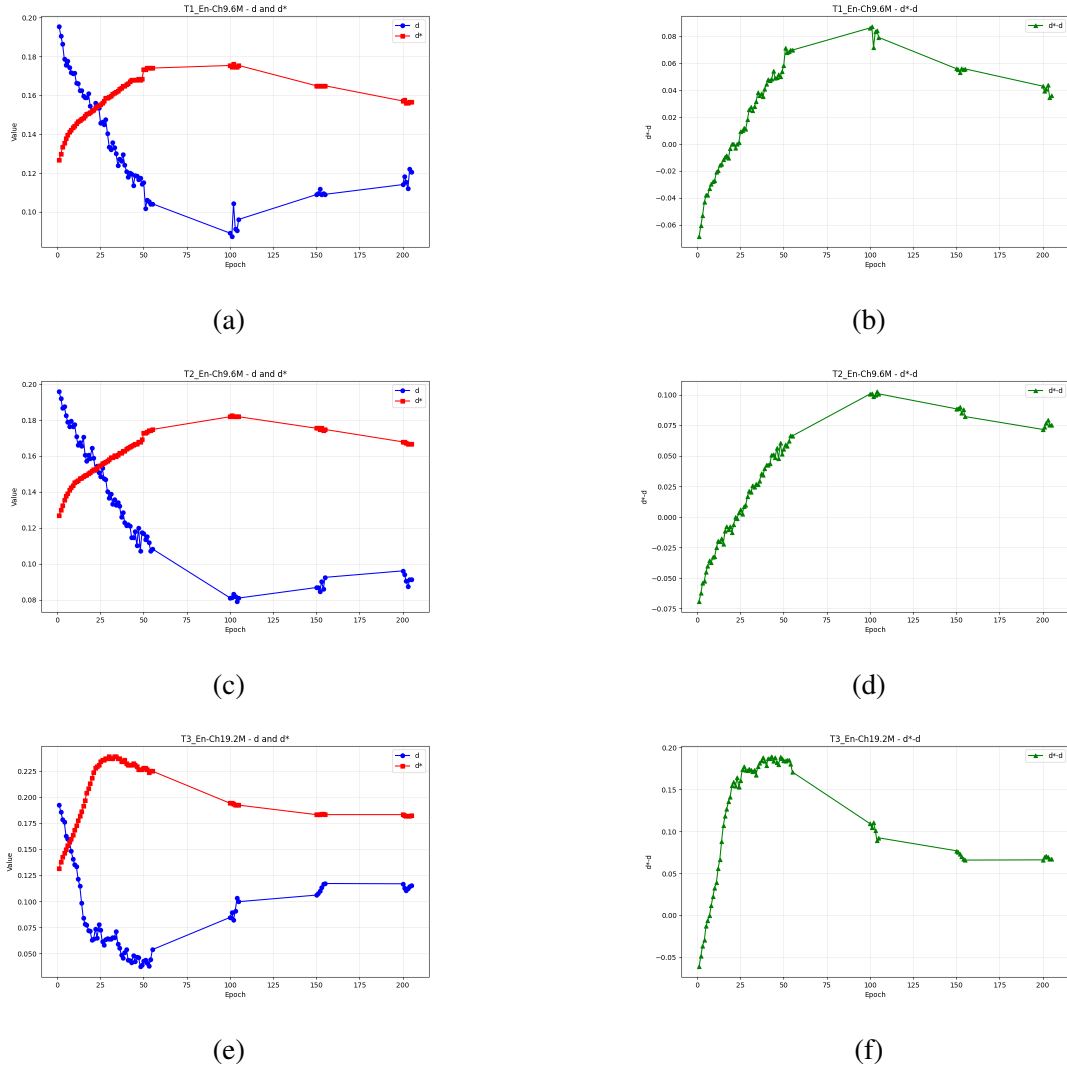


Figure 5: Evolutionary Trajectory of the Early-Stopping Metric. (a), (b), and (c) describe the variation of d and d^* with training epochs for the three models, respectively; while (b), (d), and (f) illustrate the changes in the difference between d^* and d across training epochs for these three models, respectively.

reduce training time and computational cost while preserving near-final model performance with negligible differences.

4 Conclusion

The spectral distribution of the self-attention matrix V in the initial encoder layers of Transformers is profoundly influenced by training dynamics and exhibits persistent Heavy-Tailed characteristics during the prolonged phase of stable evolution. We investigate these phenomena from multiple perspectives. Using Random Matrix Theory, we analyze the Power-Law (PL) fitting parameters and their dynamic evolution, revealing that changes in these parameters effectively reflect the progress of model training. Building upon the Heavy-Tailed Self-Regularization theory proposed by [Martin and Mahoney \(2021\)](#) and in contrast to existing spectral early-stopping methods ([Meng and Yao, 2023](#)), we partition the training process into three phases and demonstrate that the strong Heavy-Tailed phase (Phase II) constitutes a critical period for effective fine-tuning in Transformer models. This finding offers a novel perspective for understanding the internal training mechanisms of Transformers. Based on these insights, we propose a quantitative criterion for recognizing Heavy-Tailed behavior via PL fitting, which can track the formation dynamics of Heavy-Tailed structures and provide a spectral-based early-stopping criterion for Transformer models. Notably, this approach enables stopping decisions without reliance on a separate validation set.

These findings also raise several compelling questions for future exploration. For example, as Transformer architectures continue to evolve, an important direction is to evaluate whether the proposed spectral early-stopping criterion generalizes to other large language models, such as LLaMA-3 and DeepSeek-MoE. Systematic assessment of the method’s generalizability and limitations represents a crucial avenue for subsequent research. Investigating these underlying mechanisms and extending the criterion will provide significant directions for future work.

Appendix

A Theoretical Analysis of the Optimization Dynamics of the Value Matrix W^V

Recent studies (Gurbuzbalaban et al., 2021) have demonstrated that Heavy-Tailed behavior in deep neural networks is intimately linked to the optimization dynamics induced by gradient descent. In particular, Song et al. (2024) proved that, in a single-layer Transformer, optimizing only the value matrix (W^V) is sufficient to achieve the global minimum. This finding underscores the dominant and simplifying role of W^V during model training.

In practical Transformer training, however, all three attention matrices (W^Q , W^K , W^V) are jointly updated. Due to the non-convexity introduced by the softmax operation, the optimization landscapes associated with W^Q and W^K are considerably more intricate than that of W^V . To support our empirical observation that the dynamics of W^V exhibit smooth, nearly linear convergence alongside Heavy-Tailed statistical behavior, we extend existing convergence analyses-originally established for quadratic losses-to the cross-entropy loss employed in our translation tasks. Specifically, we analyze the optimization dynamics of W^V while keeping W^Q and W^K fixed.

Our objective is not to establish global convergence for the entire Transformer model but rather to demonstrate that, under mild assumptions, optimizing W^V alone follows provably stable gradient dynamics with sublinear convergence rates.

Proposition A.1. *Under the setting where only the Value matrix W^V is optimized, the loss function $f(W^V)$ satisfies:*

1. **Convexity:** f is convex with respect to W^V .
2. **Smoothness:** $\nabla_{W^V} f$ is L -Lipschitz continuous for some finite constant $L > 0$.
3. **Global Convergence:** For a learning rate $\eta \leq 1/L$, gradient descent converges sublinearly:

$$f(W_t^V) - f(W^{V*}) \leq \frac{\|W_0^V - W^{V*}\|_F^2}{2\eta t} = O(1/t),$$

where W^{V*} is an optimal solution with $f(W^{V*}) = 0$.

A.1 Setup and Notation

We consider a single-layer attention block with the standard cross-entropy loss:

$$f(W^V) = \frac{1}{N} \sum_{i=1}^N \ell(z_i, y_i), \quad \ell(z_i, y_i) = -\log(\text{softmax}(z_i)_{y_i}), \quad (\text{A.1})$$

where $z_i \in \mathbb{R}^V$ are the logits corresponding to the i -th token, and y_i is the ground-truth label.

For each input sequence X , the attention mechanism produces the logits:

$$z_i = \mathcal{A}_i(W^V) = \text{softmax}\left(\frac{Q_i K^\top}{\sqrt{d}}\right) V_i, \quad (\text{A.2})$$

where $Q_i = X_i W^Q$, $K = X W^K$, $V = X W^V$. When W^Q and W^K are fixed, the mapping $W^V \mapsto z_i$ is linear. We denote this linear operator by $\mathcal{A} : W^V \mapsto z$.

Thus the full objective can be written compactly as:

$$f(W^V) = \mathcal{L}_{CE}(\mathcal{A}(W^V), y), \quad (\text{A.3})$$

where \mathcal{L}_{CE} is convex in its first argument.

The update rule under gradient descent is:

$$W_{t+1}^V = W_t^V - \eta \nabla_{W^V} f(W_t^V), \quad (\text{A.4})$$

where $\eta > 0$ is the learning rate.

A.2 Convexity Proof

We first establish that $f(W^V)$ is convex with respect to W^V .

Lemma A.1. *(Convexity of Cross-Entropy) For a single example with logits z and label y , the loss*

$$\ell(z, y) = -\log(\text{softmax}(z)_y)$$

is convex in z .

Proof. Defining that $p_k = \text{softmax}(z)_k = \frac{e^{z_k}}{\sum_j e^{z_j}}$. The gradient is

$$\frac{\partial \ell}{\partial z_k} = p_k - \delta_{ky},$$

and the Hessian is

$$H_{kj} = \frac{\partial^2 \ell}{\partial z_k \partial z_j} = p_k (\delta_{kj} - p_j) = \text{diag}(p) - pp^\top.$$

For any vector v ,

$$v^\top H v = \sum_k p_k v_k^2 - \left(\sum_k p_k v_k \right)^2 \geq 0,$$

by the Cauchy–Schwarz inequality. Hence, H is positive semidefinite and $\ell(z, y)$ is convex in z . \square

Remark A.1. The Hessian satisfies $H\mathbf{1} = 0$ (translation invariance), hence ℓ is convex but not strongly convex.

Since \mathcal{A} is a linear operator in W^V , the composition $\ell(\mathcal{A}(W^V), y)$ remains convex. By summation over samples, $f(W^V)$ is convex in W^V .

A.3 Smoothness Proof

We next prove that $f(W^V)$ has Lipschitz-continuous gradients.

By the chain rule:

$$\nabla_{W^V} f(W^V) = \mathcal{A}^*(\nabla_z \mathcal{L}_{CE}(z(W^V))), \quad (\text{A.5})$$

where \mathcal{A}^* is the adjoint operator (matrix transpose in finite dimensions).

Since $\nabla_z \mathcal{L}_{CE}(z) = p - y_{\text{onehot}}$, the gradient w.r.t. W^V depends linearly on \mathcal{A}^* and the residual $(p - y)$.

Lemma A.2. (Smoothness) The function $\mathcal{L}_{CE}(z)$ is 1/4-smooth in z , i.e.,

$$\|\nabla_z \mathcal{L}_{CE}(z_1) - \nabla_z \mathcal{L}_{CE}(z_2)\|_2 \leq \frac{1}{4} \|z_1 - z_2\|_2.$$

Proof Sketch. The Hessian of \mathcal{L}_{CE} is $H = \text{diag}(p) - pp^\top$. All eigenvalues of H lie in $[0, 1/4]$, as proved in standard logistic regression analysis. Hence, the gradient is 1/4-Lipschitz. \square

By composition with linear operator \mathcal{A} ,

$$\|\nabla_{W^V} f(W_1^V) - \nabla_{W^V} f(W_2^V)\|_F = \|\mathcal{A}^*(\nabla_z \mathcal{L}_{CE}(z_1) - \nabla_z \mathcal{L}_{CE}(z_2))\|_F \quad (\text{A.6})$$

$$\leq \|\mathcal{A}^*\|_{\text{op}} \frac{1}{4} \|\mathcal{A}\|_{\text{op}} \|W_1^V - W_2^V\|_F. \quad (\text{A.7})$$

Thus f is L -smooth with

$$L = \frac{1}{4} \|\mathcal{A}\|_{\text{op}} \|\mathcal{A}^*\|_{\text{op}}.$$

A.4 Convergence Rate Proof

With convexity and L -smoothness established, we can apply standard convergence results.

Proposition A.2 (Convergence of W^V Optimization). *Let $f(W^V)$ be convex and L -smooth. Then, for learning rate $\eta \leq 1/L$, gradient descent satisfies:*

$$f(W_t^V) - f(W^{V*}) \leq \frac{\|W_0^V - W^{V*}\|_F^2}{2\eta t} = O(1/t).$$

Proof. The standard descent lemma for L -smooth functions gives:

$$f(W_{t+1}^V) \leq f(W_t^V) - \eta \|\nabla f(W_t^V)\|_F^2 + \frac{L\eta^2}{2} \|\nabla f(W_t^V)\|_F^2.$$

For $\eta \leq 1/L$,

$$f(W_{t+1}^V) \leq f(W_t^V) - \frac{\eta}{2} \|\nabla f(W_t^V)\|_F^2.$$

By convexity, $f(W_t^V) - f(W^{V*}) \leq \langle \nabla f(W_t^V), W_t^V - W^{V*} \rangle$. Combining and telescoping the inequality yields:

$$f(W_t^V) - f(W^{V*}) \leq \frac{\|W_0^V - W^{V*}\|_F^2}{2\eta t}.$$

□

A.5 Discussion

This analysis demonstrates that when W^Q and W^K are approximately fixed, the optimization of W^V reduces to a convex and L -smooth problem, ensuring an $O(1/t)$ convergence rate. This explains the empirically observed stability of W^V dynamics and reinforces our conclusion that the Heavy-Tailed phenomenon manifests most prominently in the value matrix.

B Pervasive Heavy-Tailed Features and Analysis of Representative Matrices

As noted by [Clauset et al. \(2009\)](#) and [Alstott et al. \(2014\)](#), even when a dataset appears to follow a power-law distribution, alternative distributions such as the exponential or log-normal may provide an equally good or even superior fit. To rigorously test this, one can compare the goodness-of-fit among competing models and compute the p-value associated with the power-law hypothesis ([Clauset et al., 2009](#); [Klaus et al., 2011](#); [Alstott et al., 2014](#)).

We compared the fits of the Power-Law, Log-Normal, and Exponential distributions to the empirical spectral distributions (ESDs) of the Q, K, and V matrices. In the English–Chinese dataset, we frequently observed that the Log-Normal distribution provided a better fit than the Power-Law—for example, fore.g., for “de.0.a.v”, “de.1.a.v”, “de.0.s.a.q”, “de.0.s.a.v”, “en.1.s.a.k”, “en.0.s.a.v”³ at epoch=1. [Alstott et al. \(2014\)](#) emphasized that when a plausible generative mechanism exists for the log-normal distribution, it often fits empirical data as well as—or better

³Here, ‘de’ denotes the decoder layer, ‘en’ denotes the encoder layer, ‘0’, ‘1’, ‘2’ indicate the layer indices, ‘a’ represents attention, ‘s.a’ refers to the self-attention layer, and ‘q’, ‘k’, and ‘v’ correspond to the Q, K, V matrix.

than—the power-law. Similarly, [Clauset et al. \(2009\)](#) observed that, unless the dataset is exceptionally large, no statistical test can reliably distinguish between the log-normal and power-law fits. Nonetheless, prior work ([Martin et al., 2021](#)) has shown that for most weight matrices, both the bulk and the tail of their ESDs can be well described by a power-law distribution. Therefore, we consider the power-law model a reasonable and theoretically grounded choice.

Despite this, we conducted direct comparisons between the power-law and log-normal distributions and obtained results consistent with those of [Clauset et al. \(2009\)](#) and [Alstott et al. \(2014\)](#). Detailed results are omitted due to space constraints. Because the exponential distribution serves as a minimal benchmark for identifying heavy-tailed behavior ([Alstott et al., 2014](#)), we further compared the power-law and exponential fits under various parameter settings using the same datasets. By examining the p-values and log-likelihood ratio R, we identified matrices for which the power-law fit significantly outperformed the exponential fit, indicating clear heavy-tailed characteristics. A summary of these results is provided in Table 5.

Table 5: Statistically Significant Heavy-Tailed Matrices

Setup	Significantly Heavy-Tailed Matrices
T1_En-Ch9.6M	en.0.s.a.v (50); de.0.s.a.q (153); en.0.s.a.q(50)
T2_En-Ch9.6M	en.0.s.a.v (50); de.0.s.a.k (100); de.0.s.a.q (200)
T3_En-Ch19.2M	en.0.s.a.v (50); en.0.s.a.q (50); en.1.s.a.q (50)

The results in Table 5 reveal a particularly consistent pattern: the `en.0.s.a.v` weight matrix persistently exhibits a superior Power-Law (PL) fit compared to the exponential fit, regardless of the dataset or architectural configuration. To further investigate this robust heavy-tailed behavior, we track the evolution of the p-value and the log-likelihood ratio (R) for this matrix across training epochs. The temporal dynamics under different experimental settings are visualized in the figure below.

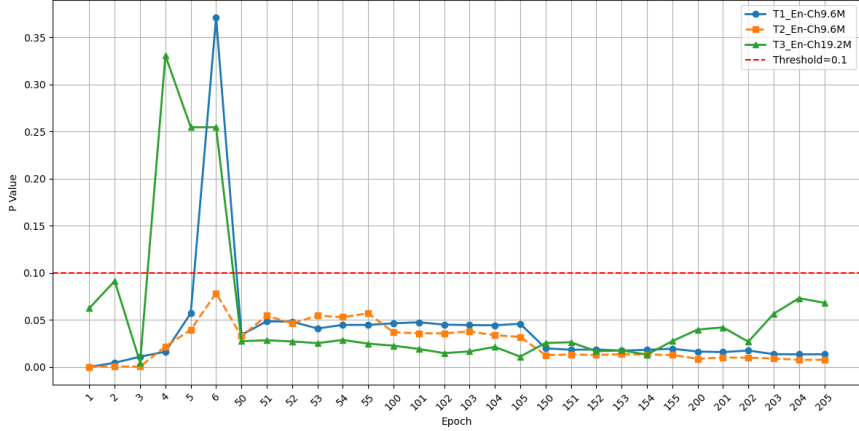


Figure 6: P-value of the power-law fit for the ‘en.0.s.a.v’ matrix versus training epoch across different experimental setups.

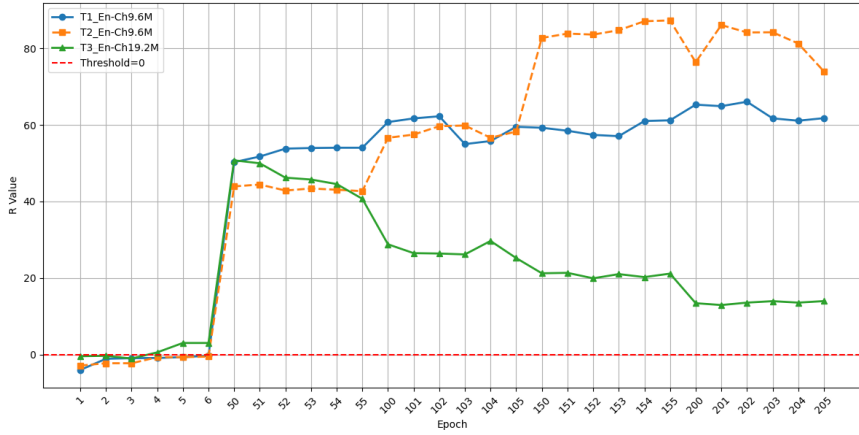


Figure 7: Log-likelihood ratio (R) for the power-law vs. exponential fit for the en.0.s.a.v matrix versus training epoch.

As evidenced by the p-values and log-likelihood ratios (R), the en.0.s.a.v matrix consistently exhibits pronounced heavy-tailed characteristics throughout training.

C Dynamic Evolution of Spectral Parameters and Training Phase Division

C.1 Workflow for Spectral Parameter Analysis of Attention Layer Matrices

On a log-log plot, a power-law distribution appears as a straight line, where the parameter α corresponds to the negative slope of this line (Clauset et al., 2009; Klaus et al., 2011; Alstott et al.,

2014; Martin and Mahoney, 2021; Yang et al., 2022). The value of α directly characterizes the distribution’s “tail heaviness”: a larger α implies a steeper slope and thus a faster decay of the distribution. To ensure a comprehensive analysis, we initially performed PL fitting on the Q, K, and V matrices from all attention mechanisms—encoder self-attention, decoder self-attention, and cross-attention. After a preliminary evaluation, we found that the spectral parameter evolution of the `en.0.s.a.v` matrix was the clearest and most consistent, whereas the Q and K matrices exhibited higher variability and layer-specific fluctuations. Based on this observation, and to further probe the essential training dynamics, we selected the spectral parameters of the V matrix as the primary indicators for subsequent analysis and for constructing the early-stopping mechanism. This choice aligns with the representative matrix analysis presented in Appendix B.

Our analysis methodology is as follows:

1. **Data Collection:** During the training of the two experimental setups (T1_Ch-En, and T2_Ch-En), we periodically extracted the Q, K and V weight matrices from all attention mechanisms at checkpoints at multiple training epochs. Specifically, matrices were extracted every 50 epochs, resulting in six sampled epochs per experiment.
2. **Matrix Construction:** For each Q, K and V matrix (denoted as \mathbf{W}), we constructed the characteristic matrix $\mathbf{X} = \mathbf{W}^T \mathbf{W}$ and applied Singular Value Decomposition (SVD) to obtain its spectral distribution.
3. **Parameter Fitting:** A power-law fit was applied to each spectral distribution. For every matrix at each sampling point, we recorded two parameters: α and x_{min} , where x_{min} represents the minimum boundary for which PL fitting can be performed, and α denotes the negative value of the slope of the function obtained after PL fitting.
4. **Data Coverage:** Since each Transformer layer contains distinct attention mechanisms (encoder self-attention, decoder self-attention, and cross-attention), we tracked all Q, K, and V matrices across layers. For example, in the 3-layer T1 model, we collected spectral parameter data from nine attention modules per checkpoint—three encoder self-attention, three decoder self-attention, and three decoder cross-attention layers.

C.2 Visual Analysis of the Evolution Process of Spectral Parameters

To perform a comprehensive multi-dimensional analysis of the dynamic evolution of the Power-Law fitting parameters (α and x_{min}), we developed a set of four complementary visualization techniques. For each of the two experimental configurations, these methods are presented in subplots

(a)–(d) of the corresponding result figures. The objective is to capture the macroscopic trends, local stability, and fine-grained fluctuations of the parameters throughout training. The visualization results for the two experimental setups are shown in Figures 8, 9, 10, and 11.

- **Raw Dynamic Observation (Subplots (a) & (c) - Raw Data Plots):** Subplots (a) and (c) directly visualize the unprocessed fitted parameters as scatter plots connected by lines over the training epochs. This provides the most immediate view of parameter fluctuations across the entire training process.
- **Macroscopic Trend Analysis (Subplot (b) - Mean Value Evolution Plot):** To capture the global convergence trends, we compute the mean values of the parameters over predefined epoch groups (e.g., epochs 1-6, epochs 50-55). Subplot (b) then plots these mean values as a function of training progress, thereby illustrating the long-term trajectory of parameter evolution.
- **Local Stability Analysis (Subplot (d) - Standard Deviation Evolution Plot):** To assess the degree of local stability, we calculate the standard deviation of the parameters within each sampling group. Subplot (d) depicts these values over time, where larger deviations indicate strong fluctuations and instability, while smaller deviations suggest convergence and stabilization of the parameters.

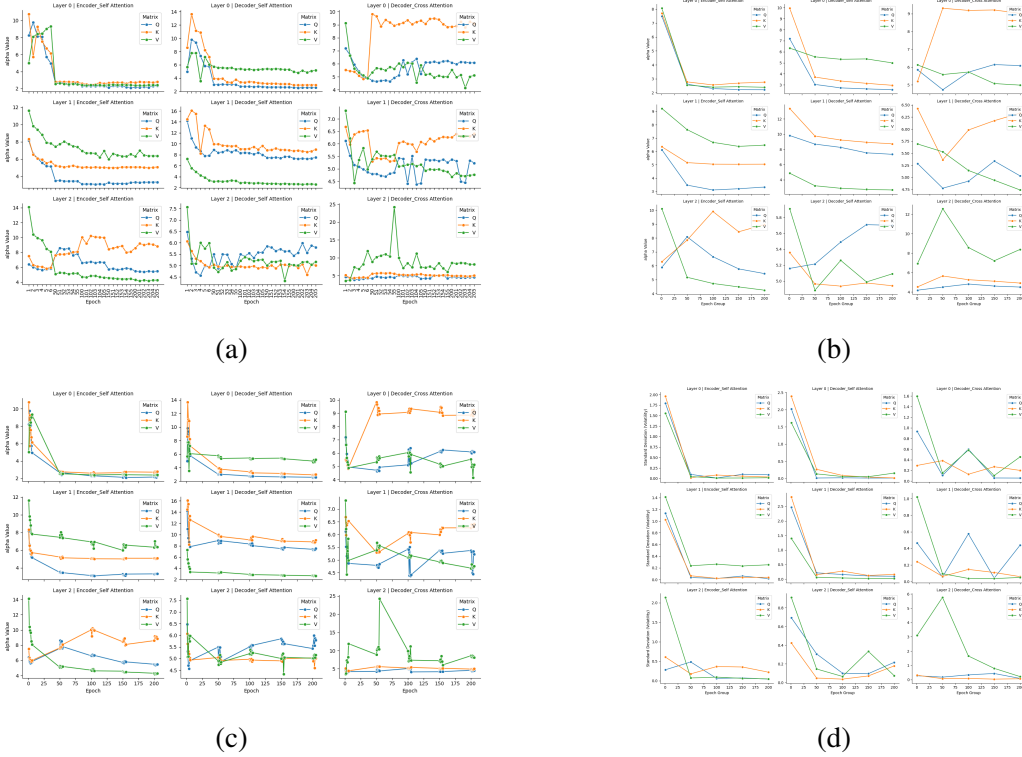


Figure 8: α parameter for T1_En-Ch 9.60M

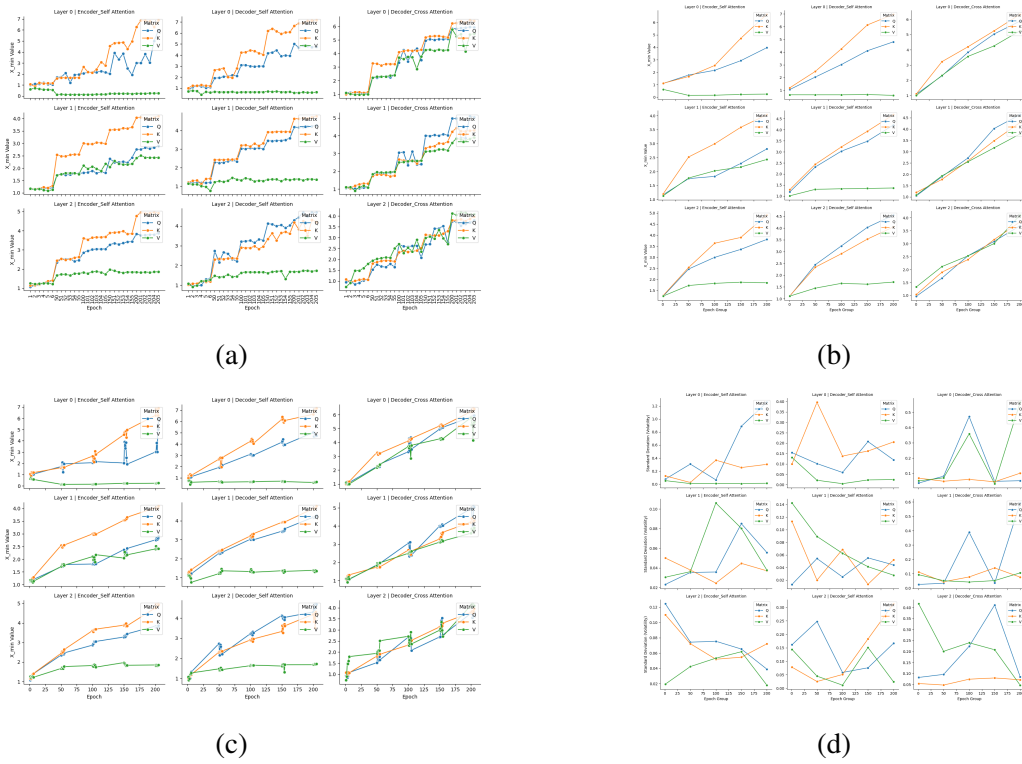
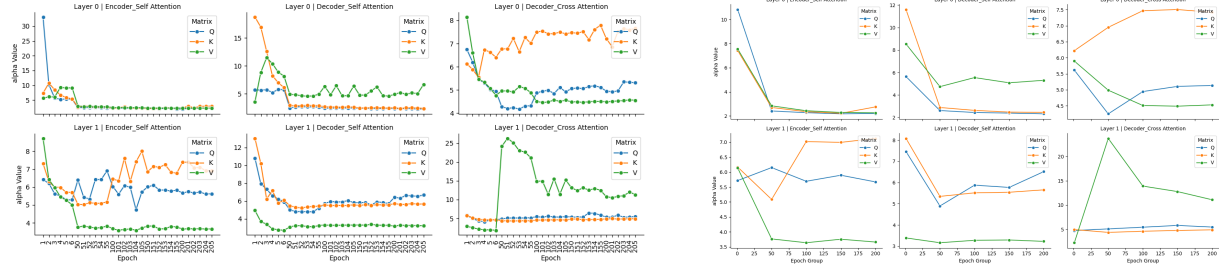
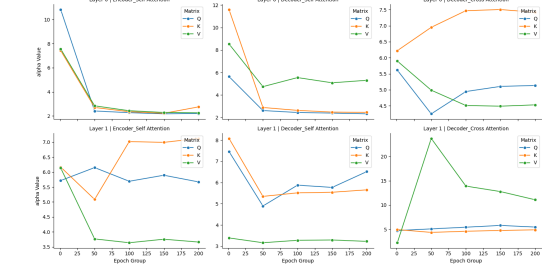


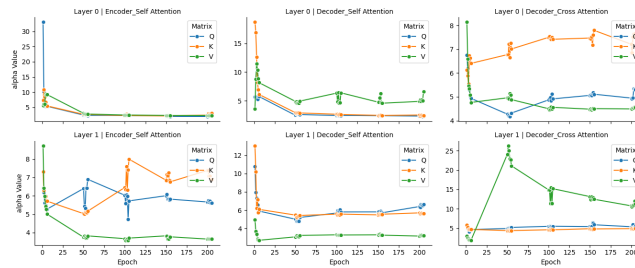
Figure 9: x_{min} parameter for T1_En-Ch 9.60M



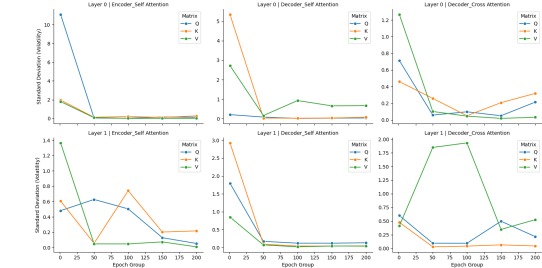
(a)



(b)

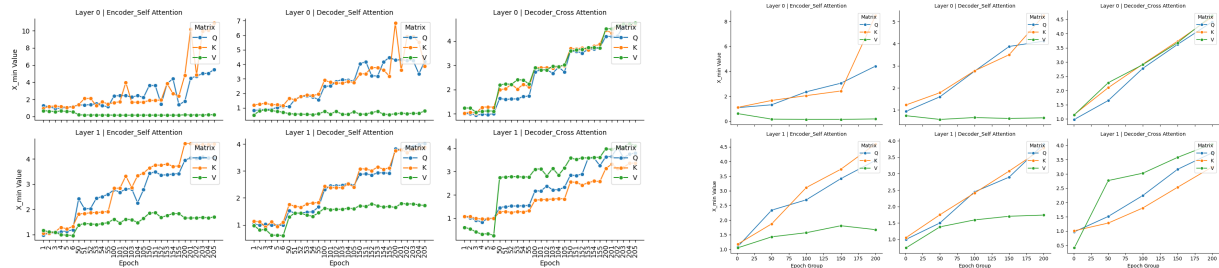


(c)

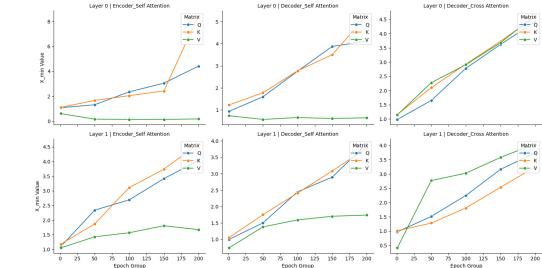


(d)

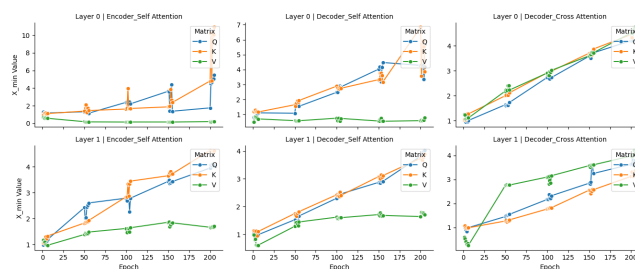
Figure 10: α parameter for T2_En-Ch 9.62M



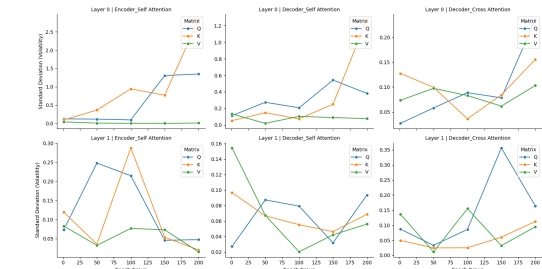
(a)



(b)



(c)



(d)

Figure 11: x_{min} parameter for T2_En-Ch 9.62M

By examining the fitted parameters α and x_{min} across the two experimental configurations, we

identify several salient patterns:

- **Shallow layers are more stable than deep layers, and the cross-attention mechanism exhibits the most significant fluctuations:** Across both the T1 and T2 models, the α trajectories of shallower layers (e.g., Layer-0) are notably smoother and more stable than those of deeper layers (e.g., Layer-1 and Layer-2) (see Figures 8 and 10). In contrast, the α values of the decoder’s cross-attention layers (Decoder-cross) display the strongest randomness and volatility throughout training. This behavior likely reflects the inherently dynamic alignment process between the source and target language representations performed by the cross-attention mechanism, leading to slower convergence of the spectral properties of its weight matrices.
- **The encoder’s self-attention layers (Encoder-self) at Layer-0 exhibit a highly consistent evolutionary pattern:** The α values fluctuate substantially during the early training phase but gradually converge thereafter. After approximately 50 epochs, the α values stabilize within the range of 2-3. A smaller α corresponds to a “heavier” spectral tail, confirming that the empirical spectral density (ESD) of the matrix exhibits a pronounced heavy-tailed behavior as training progresses.
- **The fitted x_{min} for most Q, K, V matrices shows an overall upward trend, with a few exceptions (notably, en.0.s.a.v):** An increasing x_{min} suggests that, as training advances, the power-law behavior emerges among larger eigenvalues in the spectral distribution. However, the en.0.s.a.v matrix displays a distinct downward and convergent trend. This observation highlights the special role of this shallow V matrix, which may be responsible for encoding more fundamental or global features and could be more directly associated with the model’s overall convergence dynamics.

References

Jeff Alstott, Ed Bullmore, and Dietmar Plenz. powerlaw: A python package for analysis of heavy-tailed distributions. *PLoS ONE*, 9(1):e85777, January 2014. ISSN 1932-6203. doi: 10.1371/journal.pone.0085777.

Mahya Ameryan and Lambert Schomaker. How to limit label dissipation in neural-network validation: exploring label-free early-stopping heuristics. *ACM Journal on Computing and Cultural Heritage*, 16(1):1–20, 2023.

Leonid Berlyand, Etienne Sandier, Yitzchak Shmalo, and Lei Zhang. Enhancing accuracy in deep learning using random matrix theory. *arXiv preprint arXiv:2310.03165*, 2023.

Leonid Berlyand, Theo Bourdais, Houman Owhadi, and Yitzchak Shmalo. Pruning deep neural networks via a combination of the marchenko-pastur distribution and regularization. *arXiv preprint arXiv:2503.01922*, 2025.

Aaron Clauset, Cosma Rohilla Shalizi, and Mark EJ Newman. Power-law distributions in empirical data. *SIAM review*, 51(4):661–703, 2009.

Alessandro Favero, Antonio Sclocchi, and Matthieu Wyart. Bigger isn’t always memorizing: Early stopping overparameterized diffusion models. In *The Impact of Memorization on Trustworthy Foundation Models: ICML 2025 Workshop*, 2025.

Quentin Fournier, Gaétan Marceau Caron, and Daniel Aloise. A practical survey on faster and lighter transformers. *ACM Computing Surveys*, 55(14s):1–40, 2023.

Mert Gurbuzbalaban, Umut Şimşekli, and Lingjiong Zhu. The heavy-tail phenomenon in sgd, 2021. URL <https://arxiv.org/abs/2006.04740>.

Reinhard Heckel and Fatih Furkan Yilmaz. Early stopping in deep networks: Double descent and how to eliminate it. *arXiv preprint arXiv:2007.10099*, 2020.

Jared Kaplan, Sam McCandlish, Tom Henighan, Tom B Brown, Benjamin Chess, Rewon Child, Scott Gray, Alec Radford, Jeffrey Wu, and Dario Amodei. Scaling laws for neural language models. *arXiv preprint arXiv:2001.08361*, 2020.

Andreas Klaus, Shan Yu, and Dietmar Plenz. Statistical analyses support power law distributions found in neuronal avalanches. *PLoS ONE*, 6(5):e19779, 2011. doi: 10.1371/journal.pone.0019779.

Jaris Küken, Lennart Purucker, and Frank Hutter. Early stopping tabular in-context learning. *arXiv preprint arXiv:2506.21387*, 2025.

Yassir Laaouach. HALT-cot: Model-agnostic early stopping for chain-of-thought reasoning via answer entropy. In *4th Muslims in ML Workshop co-located with ICML 2025*, 2025.

Charles H Martin and Michael W Mahoney. Implicit self-regularization in deep neural networks: Evidence from random matrix theory and implications for learning. *Journal of Machine Learning Research*, 22(165):1–73, 2021.

Charles H Martin, Tongsu Peng, and Michael W Mahoney. Predicting trends in the quality of state-of-the-art neural networks without access to training or testing data. *Nature Communications*, 12(1):4122, 2021.

Xuran Meng and Jeff Yao. Impact of classification difficulty on the weight matrices spectra in deep learning and application to early-stopping. *Journal of Machine Learning Research*, 24(28):1–40, 2023.

Tamás Miseta, Attila Fodor, and Ágnes Vathy-Fogarassy. Surpassing early stopping: A novel correlation-based stopping criterion for neural networks. *Neurocomputing*, 567:127028, 2024.

Afif Rana Muhammad, Hamzah Prasetio Utomo, Priyanto Hidayatullah, and Nurjannah Syakrani. Early stopping effectiveness for yolov4. *Journal of Information Systems Engineering & Business Intelligence*, 8(1), 2022.

Hari Kishan Prakash and Charles H Martin. Grokking and generalization collapse: Insights from htsr theory. In *High-dimensional Learning Dynamics 2025*, 2025.

Lutz Prechelt. Early stopping-but when? In *Neural Networks: Tricks of the trade*, pages 55–69. Springer, 2002.

Bingqing Song, Boran Han, Shuai Zhang, Jie Ding, and Mingyi Hong. Unraveling the gradient descent dynamics of transformers, 2024. URL <https://arxiv.org/abs/2411.07538>.

Rohan Taori, Achal Dave, Vaishaal Shankar, Nicholas Carlini, Benjamin Recht, and Ludwig Schmidt. Measuring robustness to natural distribution shifts in image classification. *Advances in Neural Information Processing Systems*, 33:18583–18599, 2020.

Dušan Variš and Ondřej Bojar. Sequence length is a domain: Length-based overfitting in transformer models. *arXiv preprint arXiv:2109.07276*, 2021.

Ashish Vaswani, Noam Shazeer, Niki Parmar, Jakob Uszkoreit, Llion Jones, Aidan N Gomez, Łukasz Kaiser, and Illia Polosukhin. Attention is all you need. *Advances in neural information processing systems*, 30, 2017.

Jingfeng Wu, Peter Bartlett, Matus Telgarsky, and Bin Yu. Benefits of early stopping in gradient descent for overparameterized logistic regression. In *Forty-second International Conference on Machine Learning*, 2025. URL <https://openreview.net/forum?id=1Z4UQ6Sz1X>.

Yaoqing Yang, Ryan Theisen, Liam Hodgkinson, Joseph E Gonzalez, Kannan Ramchandran, Charles H Martin, and Michael W Mahoney. Test accuracy vs. generalization gap: Model selection in nlp without accessing training or testing data. In *Proceedings of the 29th ACM SIGKDD Conference on Knowledge Discovery and Data Mining*, pages 3011–3021, 2023.

Yilun Yang, Ryan Theisen, Luke Hodgkinson, et al. Evaluating natural language processing models with generalization metrics that do not need access to any training or testing data. *arXiv preprint arXiv:2202.02842*, 2022.

Suqin Yuan, Lei Feng, and Tongliang Liu. Early stopping against label noise without validation data. *arXiv preprint arXiv:2502.07551*, 2025.